



1 **A morpho-tectonic approach to the study of earthquakes in Rome**

2

3 Fabrizio Marra^{1*}, Alberto Frepoli¹, Dario Gioia², Marcello Schiattarella³, Andrea
4 Tertulliani¹, Monica Bini⁴, Gaetano De Luca¹, Marco Luppichini⁵

5

6 ¹Istituto Nazionale di Geofisica e Vulcanologia, Via di Vigna Murata 605, 00143 Rome, Italy

7 ²Istituto di Scienze del Patrimonio Culturale (ISPC), Consiglio Nazionale delle Ricerche, Tito Scalo,
8 I-85050 Potenza, Italy

9 ³Dipartimento delle Culture Europee e del Mediterraneo (DiCEM), Università degli Studi della
10 Basilicata, I-75100 Matera, Italy; marcello.schiattarella@unibas.it

11 ⁴Dipartimento di Scienze della Terra, Università di Pisa, Italy

12 ⁵Dipartimento di Scienze della Terra, Università di Firenze, Italy

13

14 *corresponding author: fabrizio.marra@ingv.it

15

16 **Abstract**

17 Rome has the world's longest historical record of felt earthquakes, with more
18 than 100 events during the last 2,600 years. However, no destructive earthquake
19 has been reported in the sources and all of the greatest damage suffered in the
20 past has been attributed to far-field events. While this fact suggests that a
21 moderate seismotectonic regime characterizes the Rome area, no study has
22 provided a comprehensive explanation for the lack of strong earthquakes in the
23 region. Through the analysis of the focal mechanism and the morphostructural
24 setting of the epicentral area of a "typical" moderate earthquake (ML=3.3) that
25 recently occurred in the northern urban area of Rome, we demonstrate that this
26 event reactivated a buried segment of an ancient fault generated under both a
27 different and a stronger tectonic regime than that which is presently active. We
28 also show that the evident structural control over the drainage network in
29 this area reflects an extreme degree of fragmentation of a set of buried faults
30 generated under two competing stress fields throughout the Pleistocene. Small
31 faults and a present-day weaker tectonic regime with respect to that acting
32 during the Pleistocene explain the lack of strong seismicity and imply that a large
33 earthquake could not reasonably occur.

34



35 **Key words:** Rome; geomorphology; streambed analysis; structural geology;
36 earthquakes; seismotectonics

37

38

39

40

41

42

43

44

45

46

47 **1. Introduction**

48 On May 11th 2020, a moderate ($M_L=3.3$, $I_0=IV$ MCS) yet broadly felt earthquake
49 awoke most of the Rome's inhabitants at 05:03 a.m. (local time) (for details see
50 <https://e.hsit.it/24397691/index.html>). While producing no damage, the
51 shaking alarmed many citizens, who searched for information and reassurance
52 through the dedicated informative sources such as the INGV (Italian National
53 Institute of Geophysics and Volcanology) website. Others, instead, preferred to
54 trust on several popular beliefs which state that "Rome couldn't be struck by a
55 Big One" (i.e., a destructive earthquake with $M>7.0$), such as the mitigating effect
56 of the catacomb voids (trivial simplification from the Aristotelian theories), or
57 the protection granted by the Pope's presence. It is very likely that only few
58 people based their reactions upon a learned knowledge of the actual
59 seismotectonics features of the Rome's area. Indeed, even if a series of
60 specialized studies have been published in the last 20 years, a dedicated paper
61 investigating the reasons why Rome would not be affected by large earthquakes
62 is still missing in the scientific literature. Filling this gap is the aim of the present
63 paper in which we present a seismic study of the May 11th 2020 earthquake,
64 coupled with a statistical analysis of streambed directions in the epicentral area.
65 We identify the geometry of the seismogenic structure responsible for this $M=3.3$
66 event, and we frame it within the overall geo-morpho-structural setting of the
67 Rome's area, providing insights on the seismo-tectonic features of this region.



68

69 **2. Seismotectonic features of the Rome's area**

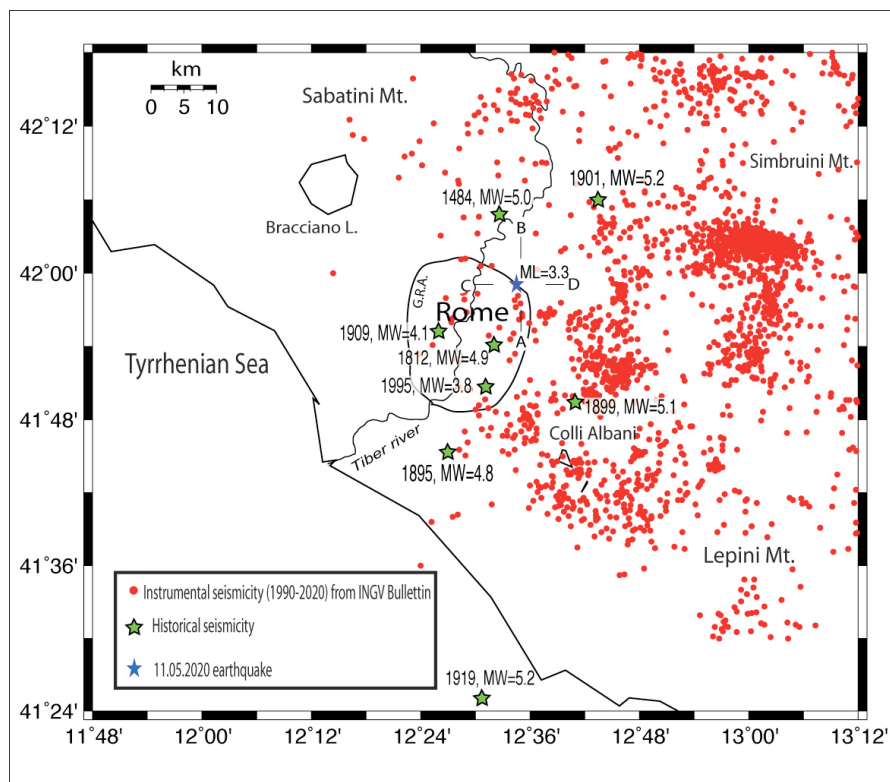
70 Our knowledge on the earthquakes that affected the roman area can be resumed
71 from the seismic catalogues' records (Guidoboni et al., 2018; Rovida et al., 2020
72 and from the literature (e.g., Tertulliani and Riguzzi, 1995; Molin and Rossi,
73 2004; Galli and Molin 2014; Tertulliani et al., 2020) as follows:

- 74 • very few events caused significant damage in the city (1349, 1703, 1915),
75 according to the studies mentioned above; all these large earthquakes
76 occurred in the Apennines mountain range;
77 • some other seismogenic areas surrounding Rome (e.g., the Colli Albani
78 Volcanic District) generated events that caused moderate damage;
79 • the greater area of Rome is periodically affected by low to moderate
80 magnitude local earthquakes which is not supposed to cause significant
81 damage.

82 A summary of the historical and instrumental seismicity of the greater area of
83 Rome is shown in Figure 1. Evidently, the completeness of our knowledge of
84 seismicity decreases going back in time. In the period of ancient Rome, as well in
85 the Early Middle Ages, strong earthquakes would seem hit Rome, sometime
86 causing damage, whose origin is still unknown. The difficulty to understand if
87 such earthquakes were generated by local or far-field sources depends on the
88 documentary accounts: the earthquake was considered a prodigy, and as such,
89 interpreted as a divine foretelling. Information on effects, damage or victims was
90 often neglected, and very rarely documented. For these reasons we are not able
91 to distinguish with reliability if such ancient events were originated, for example,
92 in the Apennines region, or near Rome.

93 It is interesting to note, from the seismic hazard point of view, that the epicenter
94 of several historical events, that occurred in the Roman countryside, are
95 nowadays included in the greater Rome territory, densely urbanized.

96 Within this limited territory we can anyway discriminate some different clusters
97 of seismicity, in particular SE and NE of the City center. Of the first cluster are
98 part the 1812, 1895, 1995 earthquakes, while the 1901 and 2020 events are
99 located NE of the city (Figure 1). Very likely this seismicity feature is due to the
100 activity of different seismotectonic structures.



101

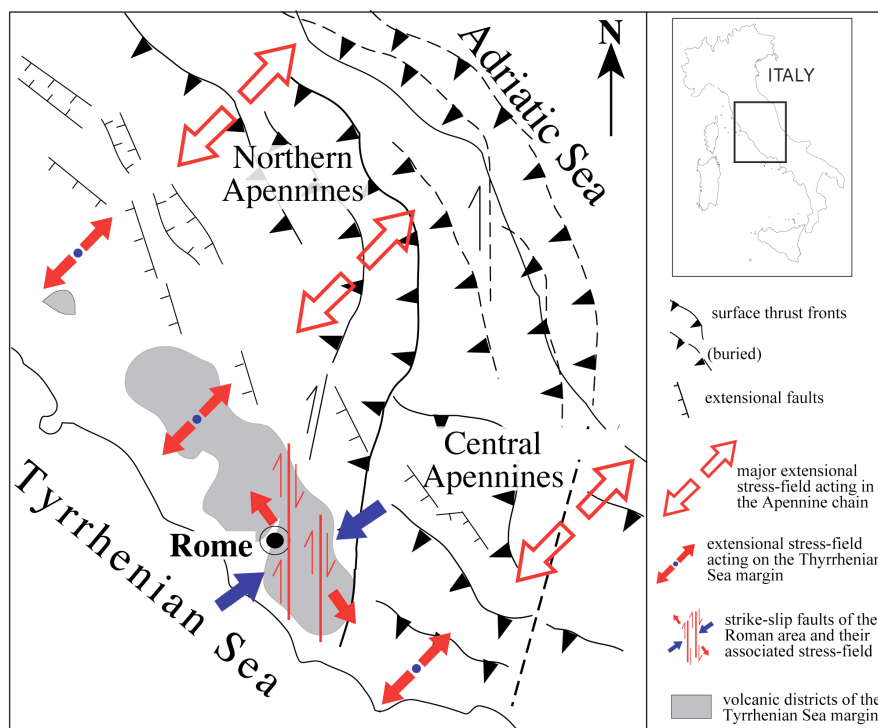
102 **Figure 1.** Map showing the seismicity of the Rome's area and mainshock location (blue star) of
103 the 11.05.2020 earthquake.

104

105

106 3. Morpho-structural features of the Rome's area

107 The morpho-structural setting of the Roman area originates in the deformation
108 of the geological substrate by combined faulting processes and erosion of rivers
109 and streams (Del Monte et al., 2016). Although partially obliterated by millennia
110 of anthropic interventions, it presents some evident and peculiar traits, whose
111 analysis allows us to understand the features of the tectonic forces (and related
112 stress-fields) that acted in the geological past through present time (Marra,
113 2001) (Fig. 2). Such analysis also consents to interpret the origin of the
114 earthquakes that nowadays affect this area.



115

116 **Figure 2.** Structural scheme of central Italy showing the competing tectonic force fields and the
117 main faults associated with them that acted in the Middle-Upper Pleistocene.
118

119

120 If we could see what the topography was like before the foundation of the City,
121 the area of Rome would appear as a large flat sector, deeply engraved and
122 dissected by the valleys of the tributary streams of the Tiber and Aniene Rivers,
123 and by the wider ones of the two main watercourses. While these features are
124 less visible in the historical center of Rome, they are still well recognizable
125 through a Digital Elevation Model (DEM) in its surrounding territory, as
126 highlighted in Fig. 3.

127



128
129 **Figure 3.** Digital elevation model (DEM) of the Roman area (TINITALY by Istituto Nazionale di
130 Geofisica e Vulcanologia (INGV), published with a CC BY 4.0 license; available at:
131 <https://doi.org/10.13127/TINITALY/1.0>), showing the strongly marked characters of the river
132 and stream incisions that form the hydrographic network afferent to the Tiber and the Aniene
133 Rivers.

134
135

136 Most of the tabular surface highlighted by the shaded area in Fig. 3 is a
137 "pyroclastic plateau" created by the emplacement of large coulter of volcanic
138 deposits. These are represented by pyroclastic flows, originated by the collapse
139 of the sustained eruptive column, and air-fall products such as windblown
140 pumice, scoria and lapilli. The deposition of these volcanic products, starting
141 from around 600,000 years ago (Marra et al., 2014; Gaeta et al., 2016), leveled
142 the ground creating a thick, layered blanket of sediments which was soon after
143 etched by the erosive action of the watercourses. The latter, however, did not
144 settle at random, but progressively shifted in correspondence with embryonic
145 fractures and fault lines created by active tectonic deformation. The same
146 fracturing and faulting associated with the extensional tectonic regime which
147 shaped the Tyrrhenian Sea margin of central Italy during the Pleistocene allowed



148 the magma residing in the mantle to rise to the surface, originating the volcanoes
149 of the so-called "Roman Province" (Peccerillo, 2017) (Fig. 2). An intense
150 seismotectonic regime must have been associated to these large extensional
151 faults, likely producing strong earthquakes throughout this region.

152

153 From the end of the Middle Pleistocene (125,000 years ago), the tectonic activity
154 began to decrease in intensity, paralleling the decrease in volcanic activity
155 (Marra et al., 2004a). Hence the seismogenic potential of the faults associated
156 with this tectonic regime must also have decreased significantly. This is one of
157 the reasons why Rome is today a low seismicity area. Moderate earthquakes
158 ($M \leq 5.0$) (Tertulliani and Riguzzi, 1995; Basili et al., 1995) are almost exclusively
159 concentrated in the volcanic area of Colli Albani (Amato and Chiarabba, 1995),
160 which is in a quiescent status (Trasatti et al., 2018). The moderate seismicity of
161 the Roman area reflects an active stress-field of the same nature, but weaker,
162 than the extensive tectonic regime that characterized the Tyrrhenian Sea margin
163 of central Italy for the entire Pleistocene, as revealed by the study of the focal
164 mechanisms of these earthquakes and borehole breakouts (Montone et al., 1995;
165 Montone and Mariucci, 2016). Such weaker tectonic regime, therefore,
166 reactivates all the faults present in this region with small movements, compatible
167 with their orientation with respect to the vectors of the stress-field (Frepoli et al.,
168 2010). The seismic events associated with this regime do not generate ground
169 ruptures, as it happens for strong, heavy damaging earthquakes, because the
170 small displacements that occur on the fault planes at depth do not propagate to
171 the surface. However, these movements repeated over time generate a slow and
172 progressive deformation of the soil, conditioning the flow direction of surface
173 waters, and exerting a "structural control" on the stream axes and alluvial valleys
174 (Marra, 2001). It follows that the hydrographic network has assumed over time a
175 geometry reflecting that of the faults occurring in the geological substrate.

176

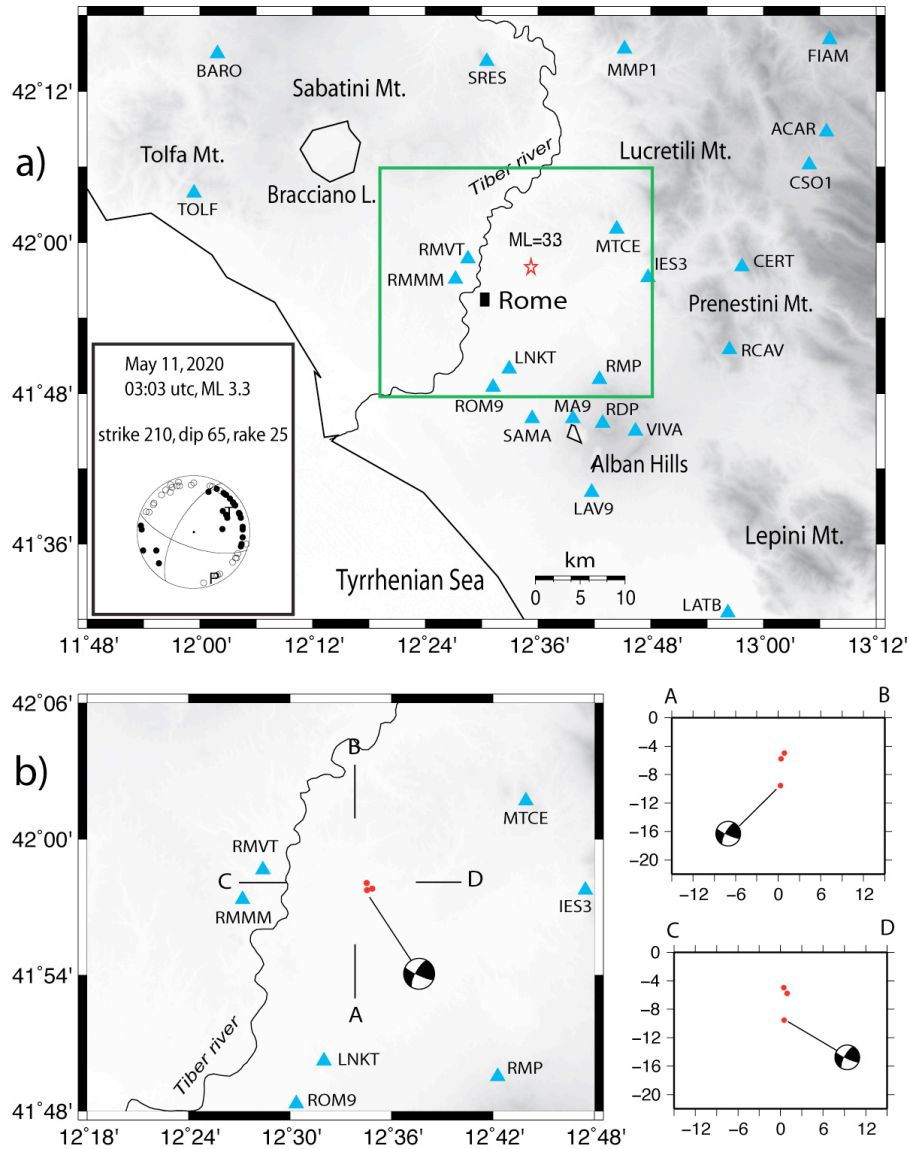
177

178 **4. Seismicity**

179 The small seismic sequence occurred on May 11th 2020 in the north-eastern area
180 of Rome was recorded by the Italian National Seismic Network (RSN) of the



181 Istituto Nazionale di Geofisica e Vulcanologia (INGV) and by the regional seismic
182 network of Lazio and Abruzzo (RSA) (De Luca et al., 2009; Frepoli et al., 2017)
183 (Figure 4). Both national and regional Italian seismic networks have been
184 significantly extended in the last two decades through installation of new three
185 components, mostly broadband, stations. In addition we integrated the dataset of
186 this sequence with the data of the Italian strong motions network (RAN) and
187 with the IESN network (Italian Experimental Seismic Network) of Central Italy,
188 an amateur seismic network equipped with very good digitizers and sensors.
189 This dense monitoring improved in the last decade the detection and location of
190 the seismicity in central Italy.
191 To accurately relocate the seismicity, we used the Hypoellipse code (Lahr, 1989)
192 and a reliable 1D V_p velocity model computed by the application of a genetic
193 algorithm (Holland, 1975; Sambridge and Gallagher, 1993). A constant value of
194 $1.84 V_p/V_s$ determined with the Wadati method (Chatelain, 1978) was used.
195



196
 197 **Figure 4.** a) Distribution of the seismic stations of the Italian National Seismic Network (RSN) of
 198 the Istituto Nazionale di Geofisica e Vulcanologia (INGV) and of the regional seismic network of
 199 Lazio and Abruzzo (RSA) used to locate the epicenter of the 11.05.2020 event (red star). b) Map
 200 and vertical distribution of the mainshock and two aftershocks.
 201

202 **5. Geomorphology**

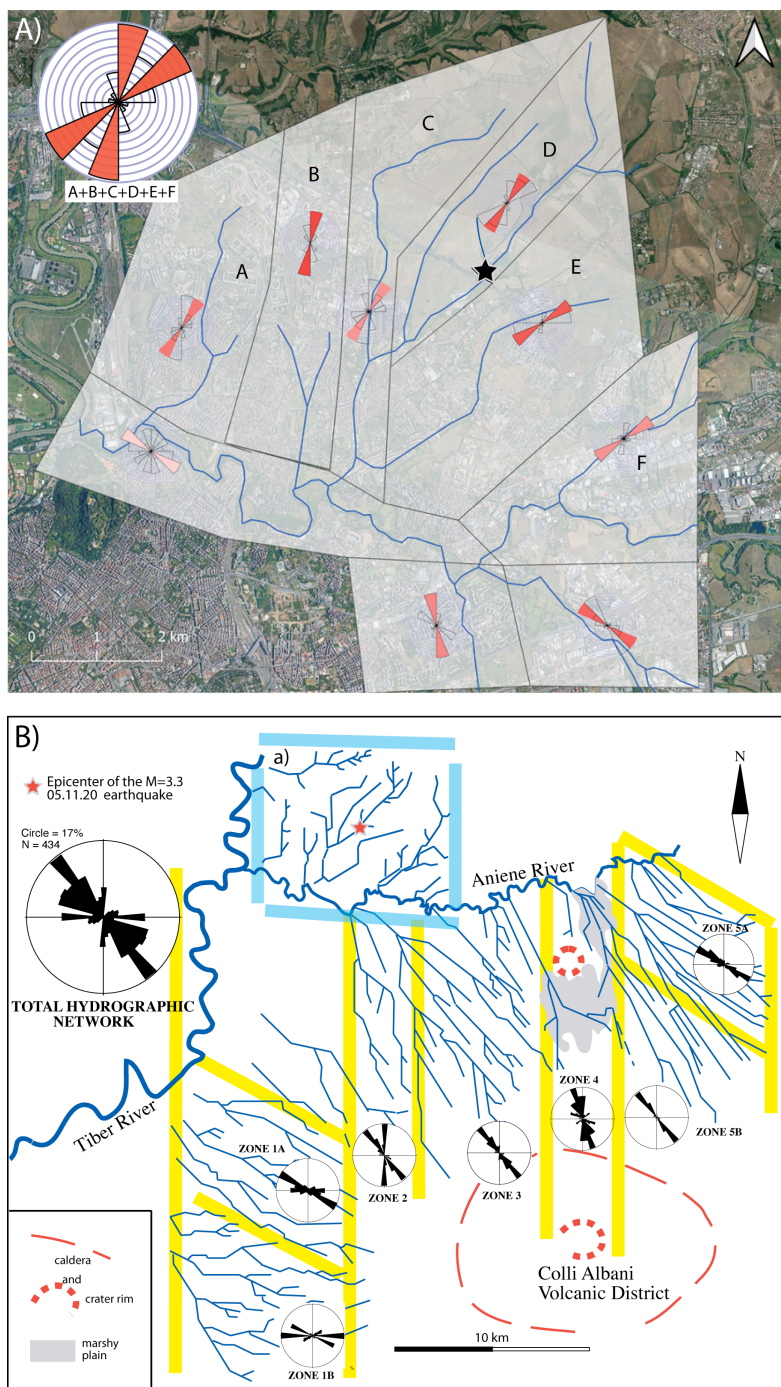
203 **5.1 Previous studies**

204 A quantitative analysis of drainage trends in the south-eastern area of Rome

205 bounded by the Tiber and Aniene Rivers and by the Colli Alabani volcanic district



206 was carried on by Marra (2001). A simple technique based on statistical analysis
207 of rectified directions of streambeds was applied (e.g., Ciccacci et al., 1987;
208 Caputo et al., 1993; Macka, 2003). Stream channel directions for the total area
209 and for different sectors were weighted according to three groups of length,
210 independent of hydrographic order, and plotted on rose diagrams.
211 While it is possible that rectifying drainage patterns can introduce directionality
212 that is unrelated to structural control, it still does indicate preferential directions
213 of river flow. In the case that these preferential directions of river flow were
214 statistically significant and different from those expected from non-structural
215 controls (e.g. topographic and geographic trends), they were interpreted to be
216 diagnostic of the structural setting. Anthropogenic intervention is also possible cause
217 of rectification of water channels, however, the linearity of the alluvial valleys
218 forming in the hydrographic network consents to compare and support the
219 directionality of the streambeds. Indeed, deep incisions and a "canyon-like"
220 morphology characterizes the alluvial plains forming the hydrographic network
221 (see Fig. 3), due to the occurrence of ca. 50 m tectonic uplift in the last 250 ka
222 (Marra et al., 2016).



223
224 **Figure 5.** A) Result of the streambed direction analysis performed in this work
225 within the hydrographic basin including the epicenter area of the May 11th event
226 (pale-blue borders in B) is compared with that performed in the south-eastern



227 Roman area, between the Tiber, the Aniene and the Colli Albani (B) (Marra,
228 2001). Analysis in the historical city center was hindered by the occurrence of a
229 widespread anthropic cover. Basemap from Qgis QuickMapServices (available
230 under [Creative Commons Attribution-ShareAlike 3.0 licence \(CC BY-SA\)](https://creativecommons.org/licenses/by/4.0/) at:
231 https://plugins.qgis.org/plugins/quick_map_services/).

232

233 Results of the analysis conducted by Marra (2001) are shown in Fig. 5B showing
234 that the NW-SE direction is the dominant one in the total area analysis (large
235 diagram in the left upper corner), as opposed to an expected radial drainage
236 trend descending from the Colli Albani caldera rim. The maximum concentration
237 of fluvial channel directions oriented N145° matches the strike of extension-
238 induced faults and fractures and agrees with the present day stress field
239 determined from focal mechanisms and breakouts data in this region (Montone
240 et al., 1995; Montone and Mariucci, 2016). Moreover, there are significantly
241 different concentrations in discrete sectors delimited by the yellow lines. In
242 particular, there are two narrow bands (zones 2 and 4) where the N-S direction
243 of the streambeds prevails, and peculiar "domains" (zones 1A, 5A) where the
244 WNW-ESE one is prevailing. The validation of the 'tectonic' hypothesis was
245 performed through comparison with geometry and kinematics of fault and
246 fractures surveyed in the area, allowing to interpret the pattern highlighted as
247 the result of a complex structural control in this area, exerted by two competing
248 stress-fields alternating each other throughout Pleistocene times (Marra, 1999,
249 2001; Frepoli et al., 2010).

250

251 **5.2 Streambed analysis**

252 In order to compare the results with previous analysis of the regional
253 deformation pattern, a quantitative analysis of drainage trends has been
254 performed in the discrete hydrographic basin located in the sector NE of the
255 Tiber and Aniene Rivers confluence (Fig. 5A), within which the May 11th
256 earthquake occurred.

257 The streambed direction analysis within the hydrographic basin including the
258 epicenter area of the May 11th event was created by using the QGIS "Line
259 Direction Histogram" plugin (Tveite, 2015), that visualizes the distribution of
260 line segment directions as a rose diagram (weighted using the line segment
261 lengths). The number of bin of direction which composes the rose diagram could
262 be set and in this work we used 8 bins corresponding to the main cardinal



263 directions. The tiles in which the area has been divided were identified
264 according to the main directions of streambeds.

265

266 **5.3 Drainage network anomalies and river profile analysis**

267 Drainage network anomalies are one of the most useful morphotectonic
268 indicators of active tectonics and they are widely used as an effective tool to infer
269 the possible control of fault activity on landscape and channels (see for example,
270 Boulton et al., 2014; Calzolari et al., 2016; Pavano et al., 2016; Kent et al., 2017;
271 Baharami, 2013). Integrated studies of possible active tectonic control on the
272 geometry of the drainage network frequently include analysis of river
273 longitudinal profiles, preferential orientation and alignments of channels, right-
274 angle confluences and fluvial elbows (Boulton et al., 2014; Pavano et al., 2016;
275 Kent et al., 2017; Gioia et al., 2018). Indeed, river profile analysis is one of the
276 most powerful tools for the identification of transient state of a drainage
277 network and recognition of knickpoints/knickzones, which represent valuable
278 and effective morphotectonic markers of recent crustal deformation (Whipple
279 and Tucker, 1999). Our approach combines the analysis of anomalies in drainage
280 network geometry (i.e. preferential orientation and/or alignments of channels,
281 fluvial elbows, right-angle confluences) with the identification of
282 knickpoints/knickzones of tectonic origin in transient longitudinal river profiles.
283 Such data have been used as morphotectonic evidences of active/recent tectonic
284 deformation induced by fault system responsible for the seismic activity of the
285 study area.

286 River profile analysis has been carried out according to the methods and
287 procedures developed by Wobus et al. (2006), Forte and Whipple (2019) using a
288 DEM with a spatial resolution of 10 m. Stream profile analysis is classically
289 carried out by identifying knickpoints or knickzones along the river longitudinal
290 profiles or by extracting a linear regression in a log-log slope-area graph, which
291 allowed us to extrapolate the concavity index (the slope of the regression) and
292 the steepness index (the y-intercept, that is the projection of the best-fit line that
293 intersects the y-axis). Knickpoints or abrupt scarps of the longitudinal profiles
294 can be related to tectonic- or eustatic- induced perturbations of ancient base-
295 levels but their formation and migration can be also related to a co-seismic fault



296 ruptures (Kirby and Whipple, 2012). In particular, the identification of fault-
297 induced disturbance on channel profiles can be performed through the
298 recognition of linear alignments of knickpoints/knickzones in channels with
299 different sizes and orientations (Boulton et al., 2014; Kirby and Whipple, 2012).
300 In order to investigate the possible occurrence of fault-related knickpoints and
301 river profile anomalies, we have investigated the river longitudinal profiles of the
302 main channels of the study area through the identification and mapping of
303 abrupt changes in river profile shape. Such data have been combined with the
304 morphotectonic analysis of the spatial distribution of drainage network
305 anomalies. Then, their spatial distribution has been used to infer the traces of
306 possible tectonic lineaments of the study area.

307

308 **6. Results**

309 **6.1 Focal mechanism and re-location of the 11 May earthquake**

310 The M_L 3.3 mainshock (11 May at 03:03 UTC) was followed over the next two
311 days by only four small aftershocks with magnitude ranging from 0.7 to 1.8.
312 Thanks to the high station coverage we were able to determine all earthquake
313 hypocenter depths with acceptable uncertainties. The average location errors
314 are 0.14 km (horizontally) and 0.32 km (vertically) with a confidence level of
315 90%. Mainshock hypocenter is at 9.6 km of depth, while the aftershock
316 hypocenters are ranging from 5.0 to 11.2 km of depth (Fig. 4). The two largest
317 aftershocks (magnitude M_L 1.8 and 1.4, respectively) have depth between 5.0
318 and 5.8 km, and are located very close to the mainshock epicenter, while the two
319 smallest aftershocks (both magnitude M_L 0.7) are located slightly towards NW
320 with respect to the mainshock epicenter, at 7.2 and 11.2 km of depth.
321 We have computed the fault plane solution of the mainshock with the FPFIT code
322 (Reasenber and Oppenheimer, 1985). First-motion polarities are 57. The focal
323 mechanism has a large strike-slip component (first nodal plane: strike 210, dip
324 65, rake 25). T-axis is oriented in a NE-SW direction according with the general
325 "Antiapennine" (NE-SW) extension. Following some tectonic information of this
326 area, the fault plane coincides with the NNE-SSW nodal plane of the solution
327 which has a left-lateral strike-slip kinematics.

328



329 **6.2 Statistical analysis of streambed directions in the epicenter area**

330 Results of the streambed analysis in the small hydrographic basin where the
331 epicenter of the May 11th earthquake occurred are summarized in Fig. 5A.
332 The streambeds in the eastern portion of the basin (discrete sectors D, E, F)
333 concentrate around the NE-SW direction, which is the one expected based on the
334 topographic gradient, perpendicular to the Aniene River course, towards which
335 the catchment basin drains. In contrast, an abrupt rotation occurs in the western
336 portion of the basin (discrete sectors A, B, C), where the streambeds are aligned
337 along the NNE-SSW direction, parallel to the main watercourse of the Tiber
338 River. Similarly to the results obtained in the southern area by Marra (2001),
339 showing that the ca. N-S direction is a characteristic feature of the streambeds in
340 this region which is clearly independent by the geographic and topographic
341 control on the hydrographic network, we interpret the N-S lineaments to reflect
342 tectonic control on the streambeds exerted by fault activity in the analyzed basin.
343 As it has been remarked in previous works (e.g., Alfonsi et al., 1991; Faccenna et
344 al., 1994, 2008; Marra et al., 2004b) strike-slip, right-lateral N-S faults have been
345 active repeatedly during the Pleistocene, up to historical times. Frepoli et al.
346 (2010) have remarked on the direct relationship between the sectors
347 characterized by N-S direction of the streambeds and seismically active fault
348 zones. It is worth noting that the May 11th earthquake epicenter occurs on the
349 northern continuation of one such N-S zone (zone 2 in Fig. 5B).

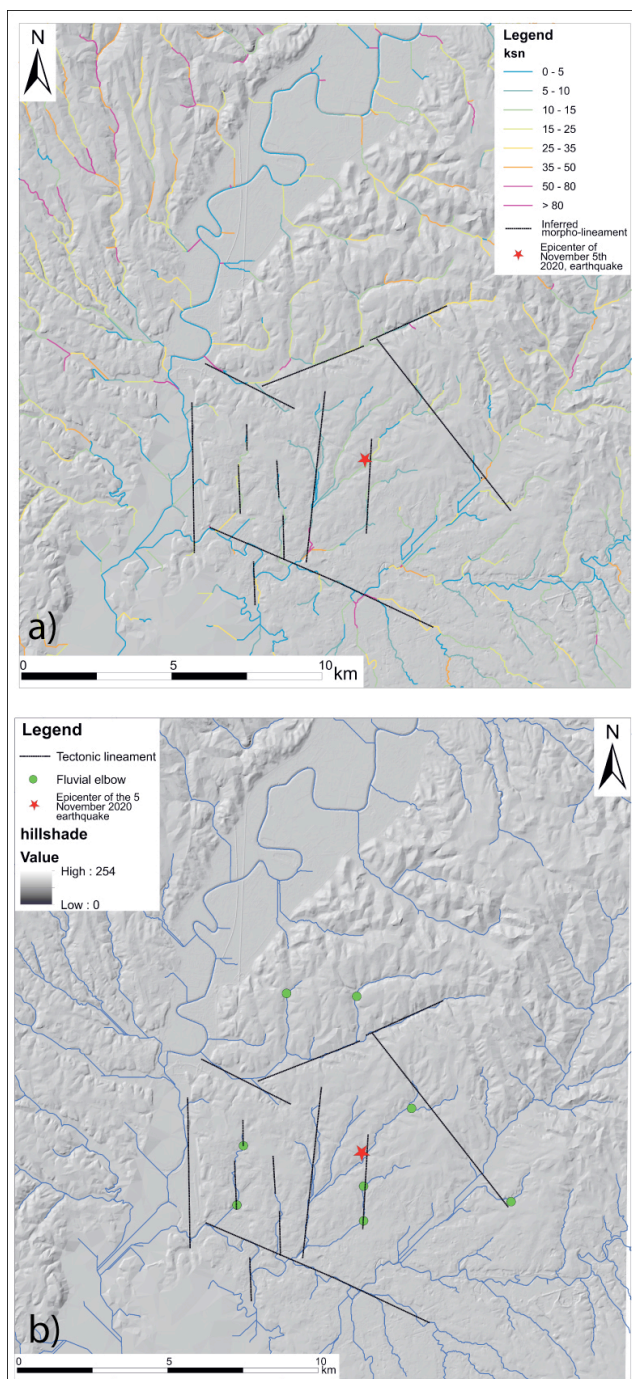
350

351 **6.3 Morphotectonic analysis of the drainage network: river profile analysis**
352 **and drainage network anomalies**

353 Analysis of longitudinal river profiles of the bedrock-rivers is based on the
354 stream power incision model (Whipple and Tucker, 1999; Wobus et al., 2006;
355 Forte and Whipple, 2019) and has been carried out to evaluate the channel
356 response to eustatic- and tectonic-induced processes. In a first step, we prepare a
357 map of the normalized steepness index (ksn) with a reference concavity index of
358 $\theta_{ref} = 0.45$ (Fig. 6a). Ksn map allowed us to perform a preliminary analysis of the
359 spatial distribution of ksn values, which can be useful to individuate the sectors
360 of the landscape featured by knickpoints and knickzones of tectonic origin.
361 Moreover, a morphotectonic map showing the spatial distribution of fluvial



362 elbows and anomalies in drainage network geometry was also introduced (Fig.
363 64b). Fig. 7 shows the results of the analysis of the river profiles, which
364 highlights how most of the channels deviates from the typical equilibrium shape
365 of the longitudinal profiles. Longitudinal profiles are featured by the presence of
366 knickpoints and knickzones, mainly in the central reach of the river profiles.
367 These knickpoints appear not controlled by lithological contact and suggest a
368 transient state of the fluvial net induced by tectonic perturbation or eustatic
369 base-level variations. In particular, we detect the occurrence of convex zones or
370 knickpoints related to a past base-levels, as testified by the presence of a large
371 “terraced surfaces” at altitude ranging from 60 to 40 m a.s.l. (Fig. 7). Our analysis
372 also reveals the occurrence of a cluster of knickpoints in the right-orographic
373 side of the Aniene River with different features than the previous ones. In fact,
374 they can be classified as slope-break knickpoint (*sensu* Wobus et al., 2006, see
375 also Kirby and Whipple, 2012) and are aligned along NW-SO and N-S orientation.
376 Such alignments as well as the location of anomalous confluences and right-angle
377 elbows of the drainage network allowed us to infer the occurrence of the tectonic
378 lineaments mapped in Fig. 7, which can be responsible for the recent tectonic
379 activity that promoted the perturbation of the fluvial net.



380
381
382
383
384

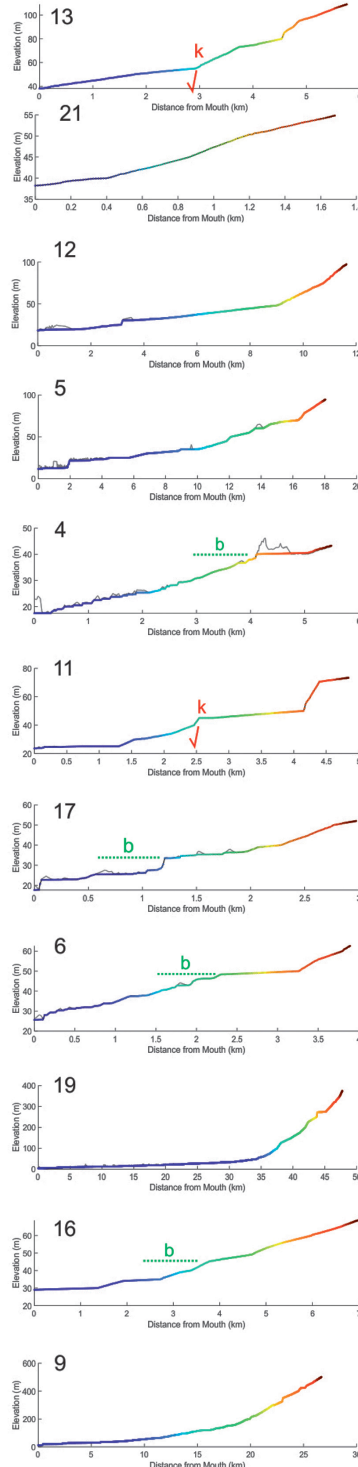
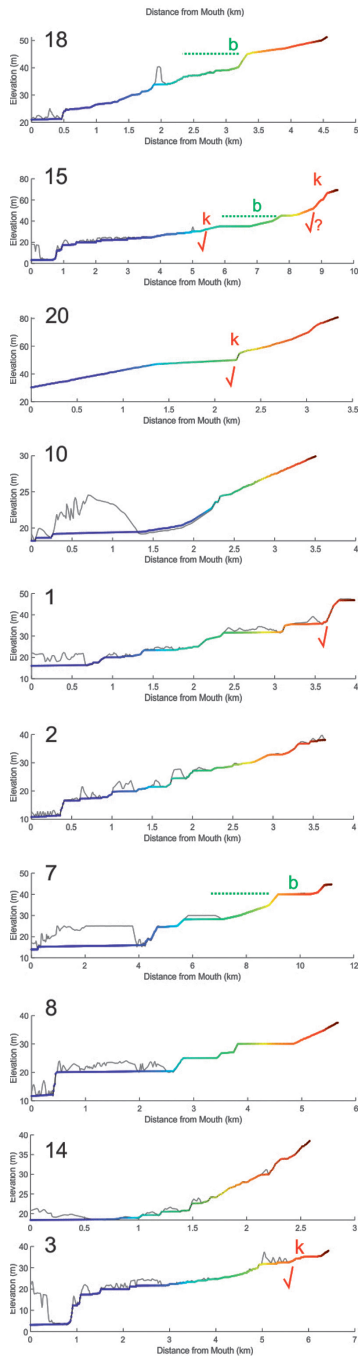
Figure 6. a) Hillshade of the study area and distribution of the normalized channel steepness index (ksn, $\theta_{ref} = 0.45$); b) Drainage network of the study area and main planar anomalies of the fluvial net. Tectonic lineaments inferred by morphotectonic analysis are also showed.



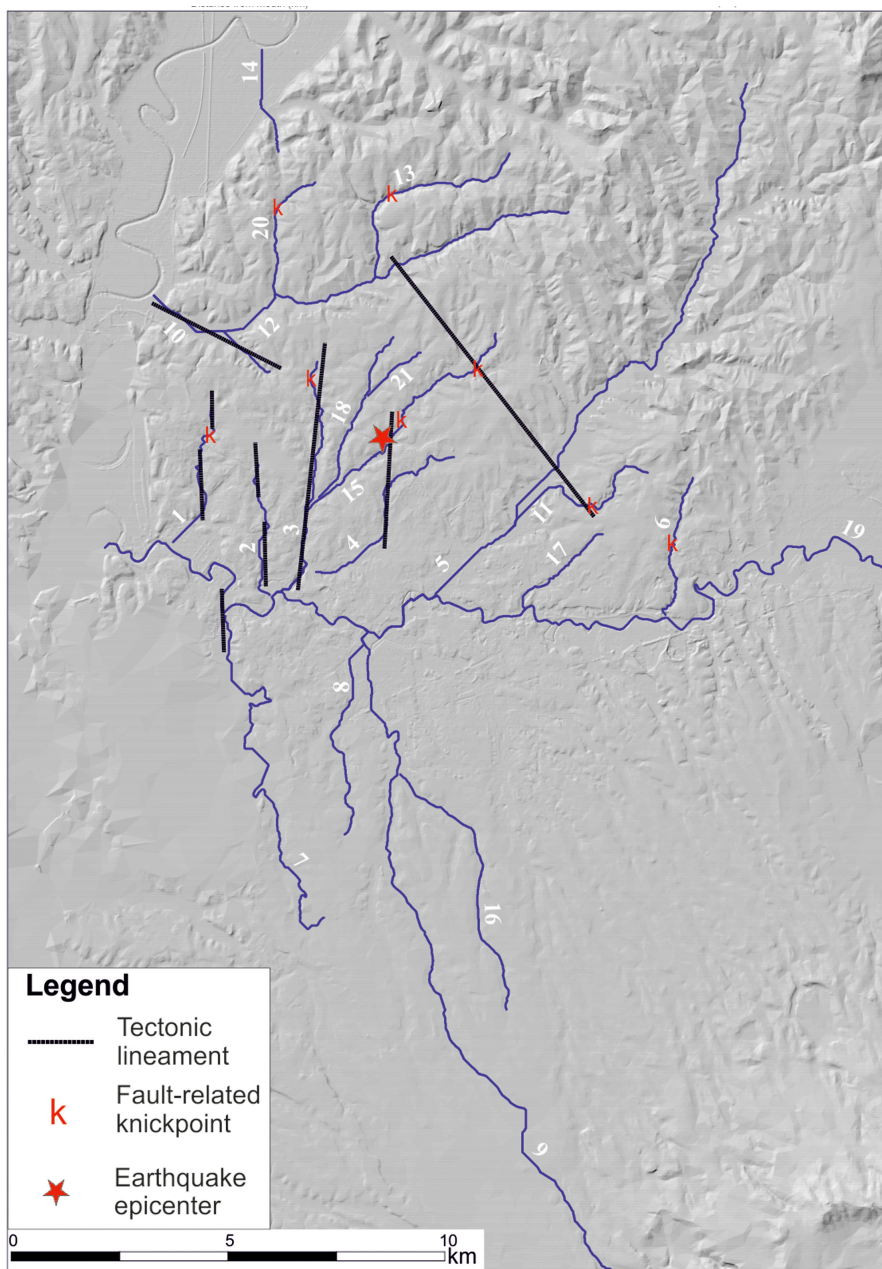
18

Symbols

- Conditioned DEM
- Unconditioned DEM
-b Knickpoint related to ancient base-level
- ↓ k Fault-related knickpoint
- ↓ k? Fault-related knickpoint (uncertain)



385



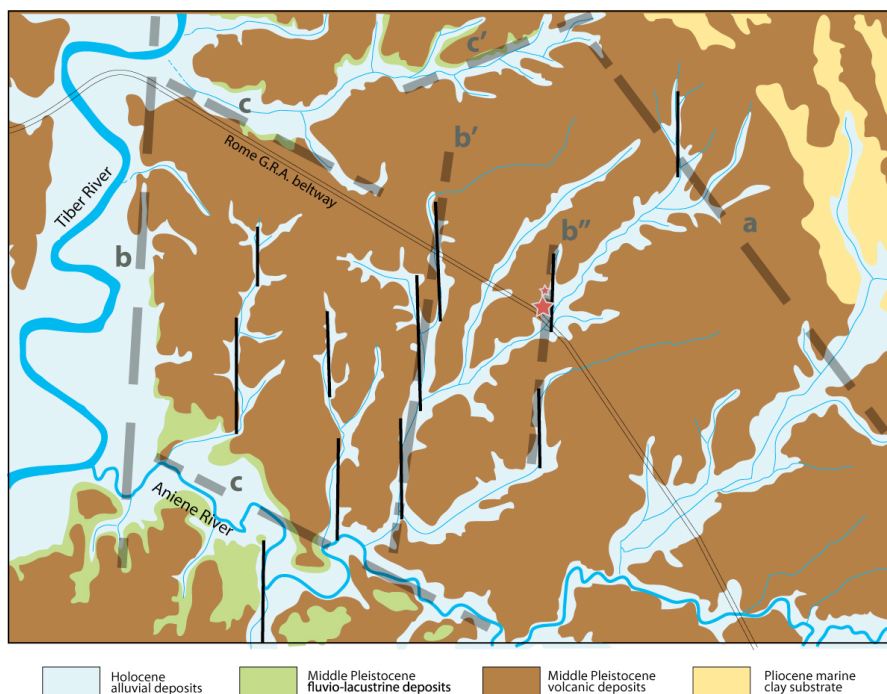
386
387
388
389
390
391
392
393
394

Figure 7. Longitudinal profiles of the main channels of the study area (location and numbering in the main map) and interpretation of the knickpoints.
DEM images in these figures: TINITALY by Istituto Nazionale di Geofisica e Vulcanologia (INGV), published with a CC BY 4.0 license; available at: <https://doi.org/10.13127/TINITALY/1.0>



395 **7. Discussion**

396 Studies conducted during the last two decades by the INGV on the geological-
397 structural and seismic-tectonic setting of the Roman area have shown that the
398 geometry of the hydrographic network reflects that of a set of buried faults
399 (Marra, 199, 2001; Frepoli et al., 2010). These are faults that are no longer active
400 with the seismic intensity they had in the geological past. They are reactivated
401 under the effect of the stress-field that currently acts in the upper crust and
402 determines the genesis of low-magnitude earthquakes in this region.
403 In particular, it has been shown that the directions of the streambeds reflect the
404 deformation field induced on the surface by the reactivation of these buried
405 faults, with a set of three preferential alignments:
406 i- The first displays an NW-SE "Apennine" direction, ("a" in Fig. 8), which
407 precisely reflects that of the large, dip-slip extensional faults that first created the
408 Tyrrhenian Sea marine basins (Barberi et al., 1994) and later, in the lower-
409 middle Pleistocene, the so-called "Tyrrhenian margin" (Fig. 2). This is a wide
410 hilly or sub-flat area between the Apennine chain and the present coast,
411 originated by the fault displacement and the "staircase" lowering of the
412 mountain relief (Parotto and Praturlon, 1975). The direction of these faults also
413 reflects the alignment of the volcanoes that developed in the Middle Pleistocene
414 along the Tyrrhenian margin, following the rise of magmas mainly along the
415 fractures in the earth's crust created by these tectonic structures (Locardi et al.,
416 1977).
417



418
419
420
421
422
423
424
425
426
427
428
429

Figure 8. Geo-morpho-structural setting of the epicenter area. The thicker dashed lines represent the main buried faults inferred from the analysis of the hydrographic network, with the exception of the "a" fault, interpreted on the basis of the presence of a structural high to the NE, represented by outcrops of Pliocene sediments. A fourth set of NE-SW lineaments is likely originated by the topographic gradient in this area and is not highlighted as potential structural control. The thin, solid lines represent the superficial expression of the deformation linked to faults that are continuous at depth (b', b''), evidenced by straight tracts of the riverbeds. One of these deep NNE-SSW faults is the one that generated the May 11th earthquake, as the focal mechanism of this event suggests.

430

431 ii- The second set of lineaments has a direction from NS to NNE-SSW ("b" in Fig.
432 8) and reflects that of even older faults, with right-lateral strike-slip character
433 (i.e. sub-vertical faults with right-hand horizontal movement (Alfonsi et al., 1991;
434 Faccenna et al., 1994). These faults are linked to the dismemberment of the
435 Apennine chain in independent arcs, due to the fragmentation of the "slab", that
436 is the "Adriatic" tectonic plate which subducted below the Apennine orogenic
437 chain (Malinverno and Rayan, 1986; Patacca et al., 1990). However, these faults
438 have been active until recent times (Faccenna et al., 2008; Marra et al., 2004b),
439 probably due to the independent geodynamic mechanism that generated them,
440 and are competing with the regime of forces that originated the extensional



441 faults (Marra, 2001; Faccenna et al., 1996). We also know from the analysis of the
442 focal mechanisms of local earthquakes that small N-S fault segments are
443 currently reactivated with opposite movement (left-lateral) together with the
444 "Apennine", dip-slip faults (Frepoli et al., 2010).

445

446 iii- Finally, a third set of lineaments has conjugated WNW-ESE and ENE-WSW
447 directions ("c" and "c'" in Fig. 8) and creates particular rhomboid "domains"⁹.
448 Within these discrete regions, the N-S direction (as in the case of the epicenter
449 area of the Rome's May 11th, 2020 earthquake, Fig. 8), or the same WNW-ESE
450 directions (sectors 1A and 5A in Fig. 5B) may prevail. The origin of these
451 domains is linked to the strike-slip faults and can be generated between two
452 long, parallel N-S lineaments (Jones and Tanner, 1995). The characteristic of the
453 strike-slip (transcurrent) faults is precisely that of being arranged in parallel
454 with "en-echelon" geometry, that is, along stairway segments which can,
455 however, locally have a lateral overlap between them (Sylvester, 1988). The en-
456 echelon geometry characterizes the surface expression of faults that are
457 continuous at depth (Sylvester, 1988) (examples b' and b" in Fig. 8).

458

459 **8. Conclusions**

460 The analysis of the hydrographic network in the epicenter area of the May 11th,
461 2020 earthquake shows a relative maximum concentration of the streambed in
462 the NNE-SSW direction: some of such rectilinear tracts, arranged with en-
463 echelon geometry, are highlighted in Fig. 5. We interpret these features as the
464 surface expression of buried NNE-SSW, strike-slip faults. Indeed, the focal
465 mechanism and aftershock alignment reveal that one of these buried ~N-S fault
466 reactivated with left-lateral movement on the occasion of the May 11th 2020
467 earthquake. Effectively, tectonically sensitive geomorphic analyses revealed the
468 occurrence of a cluster of knickpoints in the right side of the Aniene River that
469 can be classified as slope-break knickpoints and are aligned along NW-SO and N-
470 S orientation. Such a fluvial net perturbation corroborates the hypothesis of
471 recent tectonic activity affecting the study area along those faults.

472 When we consider the multitude of lineaments that are present at a wider and at
473 a smaller scale in this region (e.g., Fig. 2 and Fig. 8, respectively), we realize the



474 extreme fragmentation deriving from the intricate network of genetically
475 different faults. Such fragmentation results into a number of small fault
476 segments, with respect to the original long fault lines generated under the
477 competitive tectonic regimes that affected this region during Pleistocene times.
478 Small fault planes and a weaker tectonic regime explain the occurrence of
479 moderate seismicity and provide a likely explanation for the inhabitants of Rome
480 of the reason why they should not expect that a large earthquake may affect the
481 City.

482

483

484 **Additional information**

485 The authors declare no competing financial and non-financial interests.

486

487 **Data availability statement**

488 All data generated or analyzed during this study are included in this published
489 article.

490

491 **Author Contribution statement**

492

493 F.M. conceptualization, methodology, validation, investigation, Writing - Original
494 draft, supervision

495 A.F. methodology, validation, investigation, data curation, Writing - Original draft

496 D.G. methodology, validation, investigation, data curation, Writing - Original draft

497 M.S. methodology, validation, investigation, data curation, Writing - Original
498 draft

499 A.T. methodology, validation, investigation, data curation, Writing - Original draft

500 M.B. methodology, validation, investigation, data curation, Writing - Review and
501 editing

502 G.D.L. methodology, validation, investigation, data curation, Writing - Review and
503 editing

504 M.L. methodology, validation, investigation, data curation, Writing - Review and
505 editing

506

507

508

509

510

511



512

513 REFERENCES

514

515 Alfonsi, L., Funicello, R., Mattei, M., Girotti, O., Maiorani, A., Preite Martinez, M.,
516 Trudu, C., Turi, B.: Structural and geochemical features of the Sabina strike-slip
517 fault (Central Apennines), *Bollettino della Società Geologica Italiana*, 110, 217-
518 230, 1991.

519

520 Amato, A. and Chiarabba, C.: Earthquake occurrence and crustal structure, in:
521 *The Volcano of the Alban Hills*, edited by Trigila, R., Univ. degli Studi di Roma "La
522 Sapienza", Rome, 193–211, 1995.

523

524 Bahrami, S.: Analyzing the drainage system anomaly of zagros basins:
525 Implications for active tectonics, *Tectonophysics*, 608, 914-28, 2013.

526

527 Barberi, F., Buonasorte, G., Cioni, R., Fiordelisi, A., Foresi, L., Iaccarino, S.,
528 Laurenzi M.A., Sbrana, A., Vernia, L., Villa, I.M.: Plio-Pleistocene geological
529 evolution of the geothermal area of Tuscany and Latium, *Mem. Descr. Carta Geol.*
530 *Ital.*, 49, 77-134, 1994.

531

532 Basili, A., Cantore, L., Cocco, M., Frepoli, A., Margheriti, L., Nostro, C., Selvaggi, G.:
533 The June 12, 1995 microearthquake sequence in the city of Rome, *Ann. Geofis.*,
534 39(6), 1167–1175, 1996.

535

536 Boulton, S.J., Stokes, M., Mather, A.E.: Transient fluvial incision as an indicator of
537 active faulting and Plio-Quaternary uplift of the Moroccan High Atlas,
538 *Tectonophysics*, 633, 16-33, doi: 10.1016/j.tecto.2014.06.032, 2014.

539

540 Calzolari, G., Della Seta, M., Rossetti, F., Nozaem, R., Vignaroli, G., Cosentino, D.,
541 Faccenna, F.: Geomorphic signal of active faulting at the northern edge of Lut
542 Block: Insights on the kinematic scenario of Central Iran, *Tectonics*, 35(1), 76-
543 102, doi: <https://doi.org/10.1002/2015TC003869>2016.

544

545 Caputo, C., Ciccacci, S., De Rita, D., Fredi, P., Lupia Palmieri, E., Salvini, F.: Drainage
546 pattern and tectonics in some volcanic areas of Latium (Italy), *Geologica Romana*,
547 29, 1-13, 1993.

548

549 Chatelain, J.L.: Etude fine de la sismicité en zone de collision continentale à l'aide
550 d'un réseau de stations portables: la region Hindu-Kush-Pamir. Thèse de 3^{ème}
551 cycle, Univ. Paul Sabatier, Toulouse, 1978.

552

553 Ciccacci, S., Fredi, P., Lupia Palmieri, E., Salvini, F.: An approach to the
554 quantitative analysis of the relations between drainage pattern and fracture
555 trend, in: *International Geomorphology 1986*, edited by Gardiner, V., Proceedings
556 of the First International Conference on Geomorphology, Part II, John Wiley and
557 Sons Ltd, Chichester, 49-68, 1987.

558

559 Del Monte, M., D'Orefice, M., Luberti, G.M., Marini, R., Pica, A., Vergari, F.:
560 Geomorphological classification of urban landscapes: the case study of Rome



- 561 (Italy), *Journal of Maps*, 12, 178-189, DOI:10.1080/17445647.2016.1187977,
562 2016.
563
564 De Luca, G., Cattaneo, M., Monachesi, G., Amato, A.: Seismicity in central and
565 northern Apennines integrating the Italian national and regional networks,
566 *Tectonophysics*, 476(1), 121-135, doi:10.1016/j.tecto.2008.11.2009.
567
568 Faccenna, C., Funiciello, R., Mattei, M.: Late Pleistocene N-S shear zones along the
569 Latium Tyrrhenian margin: structural characters and volcanological
570 implications, *Bollettino di Geofisica Teorica Applicata*, 36, 507-522, 1994.
571
572 Faccenna, C., Davy, P., Brun, J.P., Funiciello, R., Giardini, D., Mattei, M., Nalpas, T.:
573 The dynamics of back-arc extension: an experimental approach to the opening
574 of the Tyrrhenian Sea, *Geophysical Journal International*, 126, 781-795, 1996.
575
576 Faccenna, C., Soligo, M., Billi, A., De Filippis, L., Funiciello, R., Rossetti, C.,
577 Tucciemei, P.: Late Pleistocene depositional cycles of the Lapis Tiburtinus
578 travertine (Tivoli, Central Italy): Possible influence of climate and fault activity,
579 *Global and Planetary Change*, 63(4), 299-308, 2008.
580 doi:10.1016/j.gloplacha.2008.06.006
581
582 Forte, A.M. and Whipple, K.X.: Short communication: The Topographic Analysis
583 Kit (TAK) for TopoToolbox, *Earth Surf Dynam*, 7(1), 87-95, doi: 10.5194/esurf-7-
584 87-2019, 2019.
585
586 Frepoli A, Marra F, Maggi C, Marchetti A, Nardi A, Pagliuca NM, et al. Seismicity,
587 seismogenic structures and crustal stress field in the greater area of Rome (Central
588 Italy). *Journal Geophysical Research* 2010;115. doi:10.1029/2009JB006322, 2010
589
590 Frepoli, A., Cimini, G.B., De Gori, P., De Luca, G., Marchetti, A., Monna, S., Montuori,
591 C., Pagliuca, N.: Seismic sequences and swarms in the Latium-Abruzzo-Molise
592 Apennines (central Italy): new observations and analysis from a dense
593 monitoring of the recent activity, *Tectonophysics*, 712-713, 312-329,
594 doi.org/10.1016/j.tecto.2017.05.026, 2017.
595
596 Galli, P.A.C. and Molin, D.: Beyond the damage threshold: the historic
597 earthquakes of Rome, *Bull Earthquake Eng.*, 12, 1277-1306,
598 <https://doi.org/10.1007/s10518-012-9409-0>, 2014.
599
600 Gaeta, M., Freda, C., Marra, F., Arienzo, I., Gozzi, F., Jicha, B., Di Rocco, T.: Paleozoic
601 metasomatism at the origin of Mediterranean ultrapotassic magmas: constraints
602 from time-dependent geochemistry of Colli Albani volcanic products (Central
603 Italy), *Lithos*, 244, 151-164, 2016.
604
605 Gioia, D., Schiattarella, M., Giano, S.: Right-Angle Pattern of Minor Fluvial
606 Networks from the Ionian Terraced Belt, Southern Italy: Passive Structural
607 Control or Foreland Bending?, *Geosciences*, 8(9), 331, PubMed PMID,
608 doi:10.3390/geosciences8090331, 2018.
609



- 610 Guidoboni, E., Ferrari, G., Mariotti, D., Comastri, A., Tarabusi, G., Sgattoni, G.,
611 Valensise, G.: CFTI5Med, Catalogo dei Forti Terremoti in Italia (461 a.C.-
612 1997) e nell'area Mediterranea (760 a.C.-1500), Istituto Nazionale di Geofisica
613 e Vulcanologia (INGV), <http://storing.ingv.it/cfti/cfti5>, 2018.
614
- 615 Holland, J.H.: *Adaptation in Natural and artificial systems*, University of Michigan
616 Press, Ann Arbor, 1975.
617
- 618 Jones, R.R. and Tanner, P.W.G.: Strain partitioning in transpression zones, *Journal*
619 *of Structural Geology*, 17, 793-802, 1995.
620
- 621 Kent, E., Boulton, S.J., Whittaker, A.C., Stewart, I.S., Cihat Alçiçek, M.: Normal fault
622 growth and linkage in the Gediz (Alaşehir) Graben, Western Turkey, revealed by
623 transient river long-profiles and slope-break knickpoints, *Earth Surface*
624 *Processes and Landforms*, 42(5), 836-52, <https://doi.org/10.1002/esp.4049>,
625 2017.
626
- 627 Kirby, E. and Whipple, K.X.: Expression of active tectonics in erosional
628 landscapes, *Journal of Structural Geology*, 44:54-75,
629 <https://doi.org/10.1016/j.jsg.2012.07.009>, 2012.
630
- 631 Lahr, J.C.: HYPOELLIPSE/Version 2.0: a computer program for determining local
632 earthquake hypocentral parameters, magnitude and first-motion pattern, U.S.
633 Geol. Surv. Open-file Report, 95, 89-116, 1989.
634
- 635 Locardi, E., Lombardi, G., Funicello, R., Parotto, M.: The Main volcanic groups of
636 Latium (Italy): relations between structural evolution and petrogenesis,
637 *Geologica Romana*, 15, 279-300, 1977.
638
- 639 Macka, Z.: Structural control on drainage network orientation an example from
640 the Loucka drainage basin, SE margin of the Bohemian Massif (S Moravia, Czech
641 Rep.), *Landform Analysis*, 4, 109-117, 2003.
642
- 643 Malinverno, A. and Ryan, W.B.F.: Extension in the Tyrrhenian sea and shortening
644 in the Apennines as results of arc migration driven by sinking of the lithosphere,
645 *Tectonics*, 5: 227-245, 1986.
646
- 647 Marra, F.: Low-magnitude earthquakes in Rome: structural interpretation and
648 implications for local stress-field, *Geophysical Journal International*, 138, 231-
649 243, 1999.
650
- 651 Marra, F., Taddeucci, J., Freda, C., Marzocchi, W., Scarlato, P.: Recurrence of
652 volcanic activity along the Roman Comagmatic Province (Tyrrhenian margin of
653 Italy) and its tectonic significance, *Tectonics*, 23, TC4013.
654 [doi:10.1029/2003TC001600](https://doi.org/10.1029/2003TC001600), 2004.
655
- 656 Marra, F., Montone, P., Pirro, M., Boschi, E.: Evidence of Active Tectonics on a
657 Roman Aqueduct System (II-III Century A.D.) near Rome, Italy, *Journal of Structural*
658 *Geology*, 26, 679-690, 2004.



- 659
660 Marra, F., Sottili, G., Gaeta, M., Giaccio, B., Jicha, B., Masotta M., Palladino, D.: Major
661 explosive activity in the Sabatini Volcanic District (central Italy) over the 800-
662 390 ka interval: geochronological - geochemical overview and
663 tephrostratigraphic implications, *Quaternary Science Reviews*, 94, 74-101,
664 DOI:10.1016/j.quascirev.2014.04.010, 2014.
665
666 Marra, F., Florindo, F., Anzidei, M., Sepe, V.: Paleo-surfaces of glacio-eustatically
667 forced aggradational successions in the coastal area of Rome: assessing interplay
668 between tectonics and sea-level during the last ten interglacials, *Quaternary*
669 *Science Review*, 148: 85-100,
670 <http://dx.doi.org/10.1016/j.quascirev.2016.07.003>, 2016.
671
672 Molin, D. and Rossi, A.: Effetti prodotti in Roma dai terremoti del 1703, in
673 *Settecento abruzzese*, in: *Eventi sismici, mutamenti economico-sociali e ricerca*
674 *storiografica*, edited by Colapietra, R., Marinangeli, G., Muzzi, P., L'Aquila, 69-106,
675 2004.
676
677 Montone, P., Amato A, Chiarabba C, Buonasorte G, Fiordelisi A., Evidence of active
678 extension in Quaternary volcanoes of Central Italy from breakout analysis and
679 seismicity, *Geophysical Research Letters* 1995;22: 1909-1912.
680
681 Montone, P. and Mariucci, M.T.: The new release of the Italian contemporary
682 stress map, *Geophysical Journal International*, 205(3),1525-1531,
683 doi:10.1093/gji/ggw100, 2016.
684
685 Patacca, E., Sartori, R., Scandone, P.: Tyrrhenian basin and apenninic arcs:
686 Kinematic relations since late Tortonian times, *Mem. Soc. Geol. Ital.*, 45, 425-451,
687 1990.
688
689 Parotto, M. and Praturlon, A.: Geological summary of the Central Apennines, in:
690 *Structural Model of Italy*, edited by Ogniben, L., Parotto, M., Praturlon A., *Quad.*
691 *Ric. Scient.*, 90, 257-311, 1975.
692
693 Pavano, F., Pazzaglia, F.J., Catalano, S.: Knickpoints as geomorphic markers of
694 active tectonics: A case study from northeastern Sicily (southern Italy),
695 *Lithosphere*, 8(6), 633-48, doi: 10.1130/L577.1, 2016.
696
697 Peccerillo, A.: *Cenozoic Volcanism in the Tyrrhenian Sea Region*, S. IAVCEI,
698 Barcelona, Springer, 2017.
699
700 Reasenberg, P. and Oppenheimer, D.: FPFIT, FPLOT and FPPAGE: FORTRAN
701 computer programs for calculating and displaying earthquake fault plane
702 solutions, *USGS Open-file Report*, 85-739, 1985.
703
704 Rovida, A., Locati, M., Camassi, R., Lolli, B., Gasperini, P.: The Italian earthquake
705 catalogue CPTI15. *Bulletin of Earthquake Engineering*, 18, 2953-2984.
706 <https://link.springer.com/article/10.1007/s10518-020-00818-y>, 2020.
707



- 708 Sambridge, M and Gallagher, K.: Earthquake hypocenter location using genetic
709 algorithms, *Bull. Seism. Soc. Am.*, 83(5), 1467-1491, 1993.
710
711 Tertulliani, A. and Riguzzi, F.: Earthquakes in Rome during the past one hundred
712 years, *Ann. Geofis.*, 38, 591–606, 1995.
713 Tertulliani A, Graziani L, Esposito A. How historical seismology can benefit from
714 bureaucracy: the case of the “Lettere Patenti” of the city of Rome in 1703. *Seism.*
715 *Res. Lett.* 2020;91, 2511-2519. <https://doi.org/10.1785/0220200046>
716
717 Trasatti, E., Marra, F., Polcari, M., Etiopie, G., Ciotoli, G., Darrah, T., Tedesco, D.,
718 Florindo, F., Ventura, G.: Coeval uplift and subsidence reveal magma recharging
719 near Rome, *Geochemistry, Geophysics, Geosystems*.
720 DOI:10.1029/2017GC007303, 2018
721
722 Tveite, H.: The QGIS Line Direction Histogram Plugin,
723 <http://plugins.qgis.org/plugins/LineDirectionHistogram/>, 2015.
724
725 Whipple, K.X. and Tucker, G.E.: Dynamics of the stream-power river incision
726 model: Implications for height limits of mountain ranges, landscape response
727 timescales, and research needs, *Journal of Geophysical Research: Solid Earth.*,
728 104(B8),17661-74, doi: 10.1029/1999JB900120, 1999.
729
730 Wobus, C., Whipple, K.X., Kirby, E., Snyder, N., Johnson, J., Spyropolou, K., Crosby,
731 B., Sheehan, D.: Tectonics from topography: Procedures, promise, and pitfalls,
732 *Special Paper of the Geological Society of America*, 55-74, 2006.
733
734